

Developing Daily Cloud-Free Snow Composite Products From MODIS Terra–Aqua and IMS for the Tibetan Plateau

Jinyuan Yu, Guoqing Zhang, Tandong Yao, Hongjie Xie, Hongbo Zhang, Changqing Ke, and Ruzhen Yao

Abstract—Daily snow cover mapping is difficult when Moderate Resolution Imaging Spectroradiometer (MODIS) snow cover products are cloud obscured. The daily cloud-free snow cover product provides an essential parameter for hydrological modeling, climate system studies, and snow-caused disaster monitoring on the Tibetan Plateau (TP). In this paper, we present an algorithm, Terra–Aqua–IMS (TAI), which combines MODIS Terra and Aqua (500 m) and the Interactive Multisensor Snow and Ice Mapping System (IMS; 4 km) to produce a daily cloud-free snow cover product (500 m). The overall accuracy of the new TAI over the TP is 94% as compared with ground stations in all-sky conditions; this value is significantly higher than the 64% of the blended MODIS Terra–Aqua product and the 55% and 50% of the original MODIS Terra and Aqua products, respectively. Without the IMS, the daily combination of MODIS Terra–Aqua can only remove limited cloud contamination: 37.3% of the annual mean cloud coverage compared with 46.6% (MODIS Terra) and 55.1% (MODIS Aqua). The resulting annual mean snow cover over the TP from the daily TAI data is 19.1%, which is much larger than the 4.7%–8.1% from the daily original MODIS Terra/Aqua and the blended Terra–Aqua snow product due to cloud blockage.

Index Terms—Cloud-removal method, Interactive Multisensor Snow and Ice Mapping System (IMS), Moderate Resolution Imaging Spectroradiometer (MODIS), snow cover, Tibetan Plateau (TP).

Manuscript received May 7, 2015; revised July 14, 2015 and August 20, 2015; accepted October 27, 2015. Date of publication November 20, 2015; date of current version March 9, 2016. This work was supported by the National Natural Science Foundation of China (41571068, 41190081, and 41301063) and Major Special Project—the China High-Resolution Earth Observation System (30-Y30B13-9003-14/16-01).

J. Yu is with the Key Laboratory of Tibetan Environmental Changes and Land Surface Processes, Institute of Tibetan Plateau Research, Chinese Academy of Sciences, Beijing 100101, China, and also with Tibet University, Lhasa 850000, China (e-mail: yujinyuan@itpcas.ac.cn).

G. Zhang and T. Yao are with the Key Laboratory of Tibetan Environmental Changes and Land Surface Processes, Institute of Tibetan Plateau Research, Chinese Academy of Sciences (CAS), Beijing 100101, China, and also with the CAS Center for Excellence in Tibetan Plateau Earth Sciences, Beijing 100101, China (e-mail: guoqing.zhang@itpcas.ac.cn; tdiao@itpcas.ac.cn).

H. Xie is with the Laboratory for Remote Sensing and Geoinformatics, University of Texas at San Antonio, San Antonio, TX 78249 USA (e-mail: hongjie.xie@utsa.edu).

H. Zhang is with the Key Laboratory of Tibetan Environmental Changes and Land Surface Processes, Institute of Tibetan Plateau Research, Chinese Academy of Sciences, Beijing 100101, China (e-mail: zhanghongbo@itpcas.ac.cn).

C. Ke is with Jiangsu Provincial Key Laboratory of Geographic Information Science and Technology, Nanjing University, Nanjing 210046, China (e-mail: kecq@nju.edu.cn).

R. Yao is with the State Key Laboratory of Remote Sensing Science, Institute of Remote Sensing and Digital Earth, Chinese Academy of Sciences, Beijing 100101, China (e-mail: yaorz@radi.ac.cn).

Color versions of one or more of the figures in this paper are available online at <http://ieeexplore.ieee.org>.

Digital Object Identifier 10.1109/TGRS.2015.2496950

I. INTRODUCTION

THE Tibetan Plateau (TP) has a mean elevation of more than 4000 m above sea level, based on the area of the plateau above 2500 m (3×10^6 km²) (Fig. 1). The TP and surrounding regions have a glacial and perennial-snow area of $\sim 100\,000$ km² comprising 46 000 glaciers [1]. The TP is also known as Asia's water tower because the melt-water from the glaciers and snow cover supplies Asia's largest rivers, which sustain the domestic water supply for more than 1 billion people downstream [2]. The station-observed air temperature changes on the TP during the past 50 years show a warming rate of 0.036 °C/year [3], which is triple the global mean surface temperature (0.011 °C/year) [4]. The warming climate may be responsible for accelerated melt of glaciers and snow on the TP and surrounding areas, which could affect water supply and water security in this region [5].

Snow plays an important role in the water budgets of high-mountain regions worldwide. In rivers originating in the high mountains of Asia, snow melt runoff accounts for a more fraction relative to glacier runoff in Yellow, Yangtze, Mekong, Salween, and Brahmaputra [6]. Snow-covered area (SCA) is also one of the key variables affecting the Earth's energy balance because of its high albedo. Additionally, accurate mapping of snow cover extent is important for agropastoral production and snow-caused disaster mitigation [7].

Snow cover has been mapped using many remote sensors in the visible, near-infrared, thermal, and microwave wavelengths. Optical remote sensing has achieved critically important data for observing the Earth's snow cover [8]–[10]. Since 1966, the National Oceanic and Atmospheric Administration (NOAA) has provided the earliest available SCA data of the Northern Hemisphere (NH) [9]. In addition, reliable hemispheric snow cover maps have been available since 1972 from NOAA's Advanced Very High Resolution Radiometer (AVHRR) sensors [11]. Snow cover extent of the NH (spatial resolution of 25 km) since 1966 has also been derived from multiple sensor combinations [12], [13]. The Landsat Multispectral Scanner System, Landsat Thematic Mapper (TM), and Landsat Enhanced Thematic Mapper Plus (ETM+) platforms have retrieved snow cover since 1973. The low temporal resolution (16 days) of Landsat data hinders its wide application in snow monitoring. Available since 2000, the Moderate Resolution Imaging Spectroradiometer (MODIS) images are superior to either Landsat, due to higher temporal resolution, or AVHRR, due to higher spatial resolution and data quality in mapping SCA [14], [15].

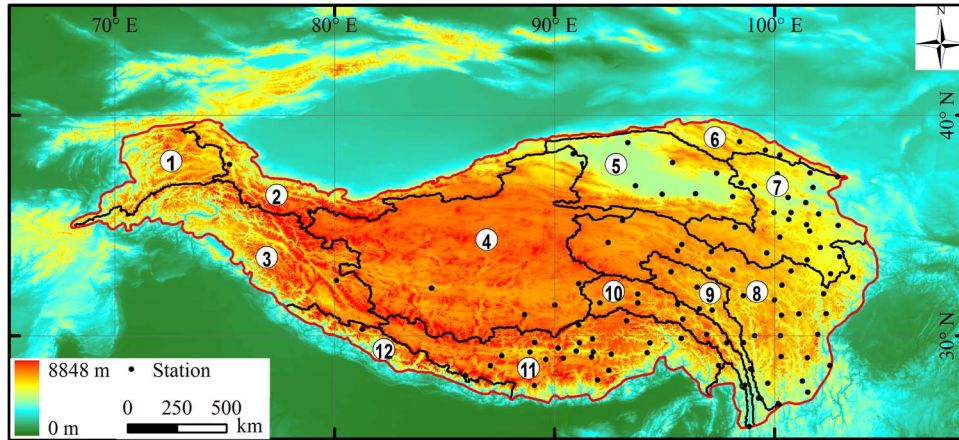


Fig. 1. Snow depth observations from 105 climate stations of the China Meteorological Administration used for validation of satellite snow cover products. The TP is divided into 12 great basins according to the large rivers and watersheds. The 12 basins are the Amu Darya (1), Tarim (2), Indus (3), Inner TP (4), Qaidam (5), Hexi Corridor (6), Yellow (7), Yangtze (8), Mekong (9), Salween (10), Brahmaputra (11), and Ganges (12) Basins.

However, cloud blockage greatly limits the application of these optical snow cover products.

Passive microwave sensors can penetrate cloud cover and provide cloud-free snow cover products. The Scanning Multi-channel Microwave Radiometer (1978–1987), Special Sensor Microwave/Imager (1987–present), and Advanced Microwave Scanning Radiometer-Earth Observation System (AMSR-E, 2002–2011) have mapped hemispheric and global-scale cloudless snow cover [10], [16]–[18]. The Interactive Multisensor Snow and Ice Mapping System (IMS) utilizes a variety of multi-sourced data sets, including visible imagery from geostationary satellites and polar orbiting satellites that include passive microwave sensors [19]. The cloud-transparent IMS data have also been extensively used for snow cover mapping; the data have a spatial resolution of 4 km (2004–present) compared with the AMSR-E resolution of 25 km [20], [21]. However, the coarse spatial resolution of passive microwave snow products relative to moderate- and high-resolution MODIS and Landsat images is a disadvantage.

Many studies have presented improved methodologies to reduce cloud obscuration and expose more snow cover pixels in the MODIS snow cover product [7], [22]–[29]. These methods include combining various MODIS Terra and Aqua products [24], [26], [27], [30], [31]. The multisensor combinations utilize the high temporal resolution of MODIS snow products and the cloud transparency of passive microwave data, such as AMSR-E [25], [26], [32]. In addition, spatial filtering [27], [30], [33] and temporal filtering [27], [28], [30], [34] are applied to neighboring cloud-free pixels (in space and time) to replace cloud-covered pixels. A zonal snowline approach employs the snowline threshold for a given zone to label the cloud pixels above this threshold as snow [27], [31], [35]. In contrast, the MODSCAG algorithm (MODIS SCA and Grain Size) relies on the relative shape of the snow's reflected solar radiation spectral response to accurately characterize the fractional snow cover [36]–[39].

Combining MODIS Terra–Aqua (500 m) with the IMS (4 km) can create daily cloud-free snow cover images with higher spatial resolution than is obtainable from the IMS alone.

In this paper, an algorithm is developed to combine MODIS Terra–Aqua and IMS (TAI) and to automatically generate daily cloudless snow cover data on the TP. The performance of TAI is evaluated with the station-based snow depth measurements. The TP is divided into 12 great basins to compare the performance of snow cover mapping from different products (Fig. 1).

II. DATA USED

A. Station-Based Snow Depth Data

The remoteness, high altitude, and harsh weather conditions complicate the fieldwork on the TP. The China meteorological stations were established in the 1950s, and they record snow depth data (in centimeter), along with other meteorological data such as temperature and precipitation. Most of the TP stations are located in the east ($> 90^\circ$ E) at low elevations (< 4800 m; Fig. 1). For this study, daily *in situ* measurements of snow depth from 105 China Meteorological Data (CMA) climate stations between 2001 and 2010 are obtained from the CMA Sharing Service System (<http://cdc.cma.gov.cn>). Snow depth data from CMA stations are rounded to the nearest centimeter. These data are quality controlled and verified manually and are used to validate snow cover obtained from remote sensing data.

B. MODIS Snow Cover Products

The Earth Observing System Terra and Aqua satellites, including the MODIS instruments, were launched in December 1999 and May 2002, respectively (Table I). MODIS Terra crosses the local equator at approximately 10:30 A.M. in a descending node; Aqua crosses the equator at 1:30 P.M. in an ascending node, both with a sun-synchronous near-polar circular orbit. The MODIS snow-mapping algorithm employs a normalized difference snow index (NDSI) with bands 4 and 6 (7 for Aqua) to differentiate snow and no-snow features [40]. MODIS standard snow products are produced at a spatial resolution of ~ 500 m with nominal swath coverage of 2330 km by 2330 km in both daily products and 8-day composite product.

TABLE I
SATELLITE SNOW COVER DATA USED IN THIS STUDY

Snow cover product	Sensor	Spatial resolution	Temporal resolution	Nominal data array dimensions	Date started available	Map projection	Algorithm
MYD10A1	MODIS /Aqua	500 m	daily	1200 km × 1200 km	Jul 4, 2002	Sinusoidal	NDSI
MOD10A1	MODIS /Terra	500 m	daily		Feb 24, 2000		
MOD10A2	MODIS/Terra	500 m	8-day		Feb 26, 2000		
IMS	Multiple sensors	4 km	daily	6144 km × 6144 km	Feb 23, 2004	Polar stereographic projection	Automated snow mapping algorithm

MODIS standard snow products, such as MOD10A1 and MOD10A2, highly agree (> 90%) with *in situ* measurements in clear-sky conditions and snow depths > 4 cm [41]–[43], although the accuracy decreases in the transitional periods of accumulation and melt [39], [44] and sparse snow conditions [36].

However, an evaluation of MODIS standard snow cover product in northern Xinjiang indicates that overall accuracy can go below 40% in all-sky conditions, i.e., cloud-covered and cloud-free conditions [45]. In the many studies mentioned previously, the 8-day standard MODIS snow products (of low cloud cover) are preferred, but the 8-day composites have a reduced temporal resolution. Developing a daily cloud-free snow cover product is useful for providing more frequent observations of snow cover on the vast high plateau.

In this paper, daily MODIS Terra/Aqua (MOD10A1/MYD10A1; MODIS Terra/Aqua Snow Cover Daily L3 Global 500 m SIN GRID V005) and 8-day MODIS Terra (MOD10A2) over 2001–2013 are acquired (<http://reverb.echo.nasa.gov/reverb/>) [46]. Eight MODIS tiles (H23V05, H24V05, H24V06, H25V05, H25V06, H26V05, H26V06, and H27V06) are downloaded to cover the entire TP. If a missing day is found in either Terra or Aqua, the merged Terra–Aqua data on this day are not produced. We only use the 8-day MODIS Terra in this study because the Terra snow product provides superior snow mapping and fewer cloud cover images than Aqua [22], [47].

C. IMS Data

NOAA/NESDIS has operated the IMS since 1997; it has a nominal resolution of 24 km at the daily time scale and covers the NH (1024 by 1024 grids) in a polar stereographic projection [48], [49]. The IMS data set blends various snow products, including those derived from visible and infrared sensors and passive microwave sensors on various satellites and other ancillary data [20]. The IMS product estimates global SCA every day, regardless of the presence of clouds. The pixel values of the IMS are coded as 1 for sea/lake, 2 for land, 3 for sea/lake ice, 4 for snow, and 0 for outside the NH. The data file is stored in ASCII or GeoTIFF format. The IMS has been widely used for snow cover mapping and climatological analysis of large-scale snow extents [19], [50]. Since February 23, 2004, the IMS has been distributed at a pixel size of 4 km. The IMS snow cover images (4-km resolution and 6144 by 6144 grid) are downloaded (<http://nsidc.org/data/g02156>) [51] and used in this study.

III. METHODS

A. Multisensor Combination of MODIS Terra–Aqua and IMS (TAI)

Fig. 2 shows a detailed flowchart of data processing and the integration of MODIS Terra, Aqua, and IMS. The MODIS Reprojection Tool is used to reproject MODIS data from the original 463.3 m in a Sinusoidal Projection into a 500-m Albers Equal-Area Conic Projection with the WGS84 datum. The eight MODIS tiles covering the entire TP are mosaicked and converted to GeoTIFF files. The original MODIS snow image is a coded raster: 0 (data missing), 1 (no decision), 11 (polar), 254 (saturated MODIS sensor detector), 255 (no data), 39 (ocean, which is not the case on the TP), 37 (water), 25 (land), 50 (cloud), 100 (lake ice), and 200 (snow).

The first combination is to produce daily merged Terra–Aqua images based on daily MODIS Aqua and Terra snow products, using a priority scheme [22]. The snow pixel has the highest priority, and cloud has the lowest priority. The cloud-covered pixels in the MODIS Terra (Aqua) image are replaced with the MODIS Aqua (Terra) values if cloud-free in the Aqua (Terra) image; otherwise, no change is made if cloud cover is in both images. The second combination is to produce a daily combined Terra–Aqua–IMS (TAI). The IMS data are resampled from 4 km to 500 m to integrate the daily blended MODIS Terra–Aqua. The composite rule is that the remaining cloud pixels (code 50) of Terra–Aqua images are replaced with IMS pixel values and then remapped to MODIS value codes, i.e., IMS 1 to TAI 37, IMS 2 to TAI 25, IMS 3 to TAI 100, and IMS 4 to TAI 200, while other types of pixel values in Terra–Aqua remain the same in TAI because MODIS has a higher spatial resolution than the IMS. The same rule is also applied to a value of 0 of the Terra–Aqua images when combined with the IMS to produce the TAI images (Fig. 2).

B. Evaluation of Snow Cover Products

The daily MODIS Terra and Aqua, daily combined MODIS Terra–Aqua, and daily TAI products are compared with ground-based measurements of snow depth, for snow accuracy and overall accuracy in both clear-sky and all-sky (cloud-covered and cloud-free) conditions [23], [30], [42], [43]. Snow accuracy in clear-sky (S_c) or all-sky (S_a) condition is defined as the number of days when snow cover is observed by both climate station and satellite divided by the total number of days with snow cover seen at stations in clear-sky (1) or all-sky

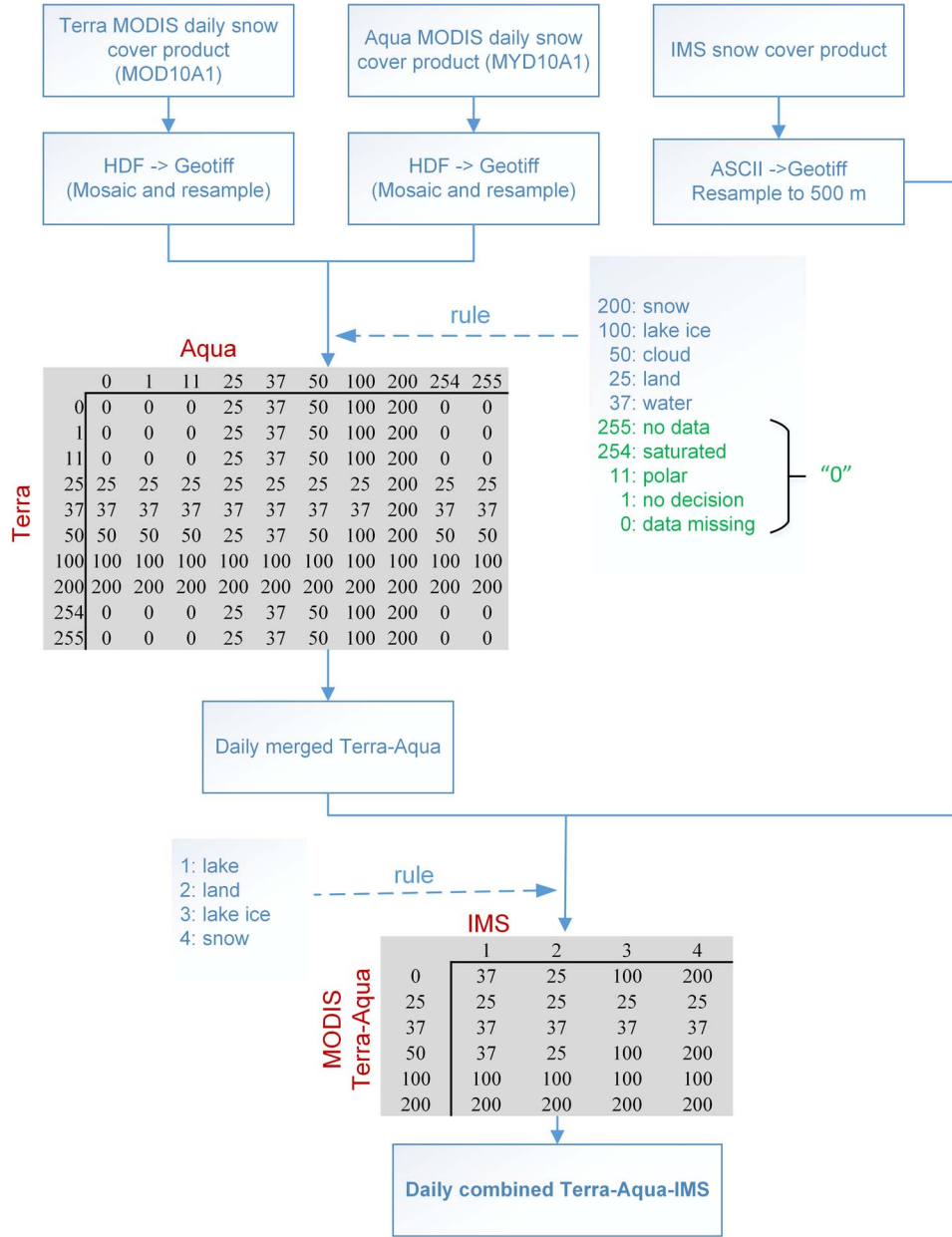


Fig. 2. Flowchart showing the combining processes for the daily MODIS Terra and Aqua and IMS (TAI).

condition (2). The overall accuracy in clear-sky (O_c) or all-sky (O_a) condition is defined as the number of days with snow cover or no-snow cover seen by both stations and satellite divided by the total number of station observations in clear-sky (3) or all-sky condition (4) (Table II)

$$S_c = \frac{a}{a+b} \quad (1)$$

$$S_a = \frac{a}{a+b+e} \quad (2)$$

$$O_c = \frac{a+d}{a+b+c+d} \quad (3)$$

$$O_a = \frac{a+d}{a+b+c+d+e+f} \quad (4)$$

where a , b , c , d , e , and f in (1)–(4) represent the number of station observations in each particular classification category as described in Table II.

TABLE II
CONFUSION MATRICES FOR SATELLITE SNOW DATA COMPARED
WITH STATION-BASED SNOW OBSERVATIONS

Climate station	Satellite snow cover		
	Snow	No-snow	Cloud
Snow	a	b	e
No-snow	c	d	f

IV. RESULTS AND DISCUSSION

A. Accuracy Assessment of Snow Cover Products

The resultant snow cover maps are evaluated with *in situ* measurements of snow depth. Table III shows the snow and overall accuracies in both clear-sky and all-sky conditions for MODIS Terra (Aqua), merged MODIS Terra–Aqua, and TAI between 2001 and 2010. The snow accuracies of MODIS snow products in clear-sky conditions at the snow depth of ≥ 1 cm are

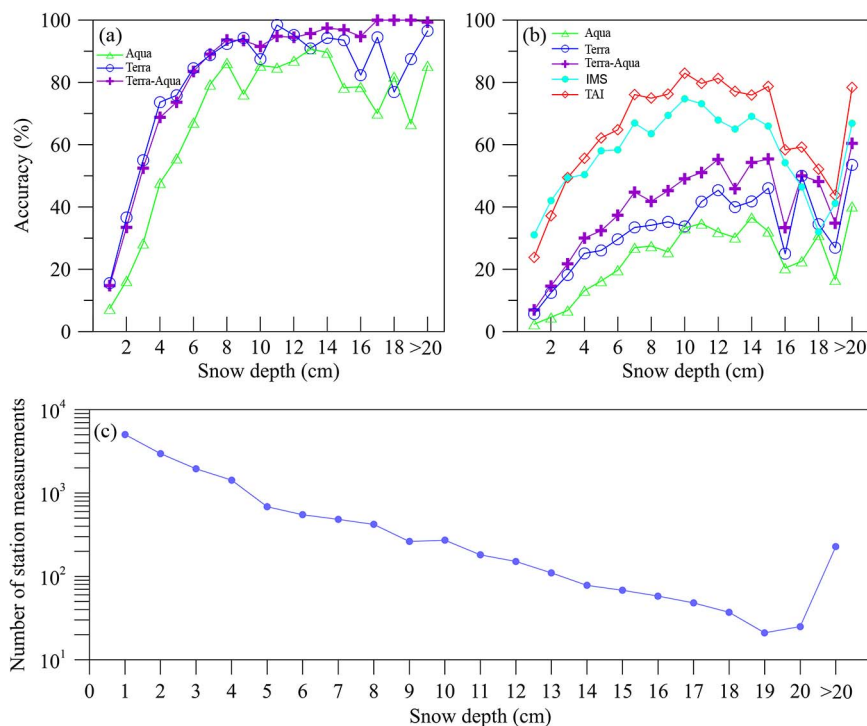


Fig. 3. Comparison of snow accuracy in (a) clear-sky and (b) all-sky conditions between the remote sensing image and *in situ* snow depth data. (c) Log number of station measurements for snow depth from 105 CMA stations between 2001 and 2010. Remote sensing data include the daily MODIS Terra and Aqua, daily combined MODIS Terra–Aqua, IMS, and daily cloud-free TAI. Station locations are shown in Fig. 1.

TABLE III

COMPARISON OF SNOW ACCURACIES IN CLEAR-SKY (S_c) AND ALL-SKY CONDITIONS (S_a) AND OVERALL ACCURACIES IN CLEAR-SKY (O_c) AND ALL-SKY CONDITIONS (O_a) AMONG SNOW PRODUCTS OF THE DAILY MODIS TERRA/AQUA, DAILY COMBINED TERRA–AQUA, AND DAILY TAI OVER THE PERIOD 2001–2010. SNOW DEPTHS OF ≥ 1 cm (4 cm)

FROM CMA STATIONS ARE USED. VALUES IN PARENTHESES DENOTE ACCURACY AT THE SNOW DEPTH OF ≥ 4 cm

	S_c (%)	S_a (%)	O_c (%)	O_a (%)
MODIS Terra	46 (84)	16 (31)	97 (98)	55 (56)
MODIS Aqua	31 (69)	9 (22)	96 (98)	50 (51)
Combined Terra–Aqua	45 (83)	20 (39)	96 (98)	64 (65)
IMS	-	45 (60)	-	91 (92)
TAI	-	43 (67)	-	94 (95)

31%–46%, which is greater than their accuracies of 9%–16% in all-sky conditions. The cloud-free IMS has an accuracy of 45% in all-sky conditions. The cloud-removed TAI shows an improved accuracy (44%) in all-sky conditions compared with MODIS Terra/Aqua and Terra–Aqua combination. The overall accuracies for the MODIS snow cover products in clear-sky conditions present a significant increase ($\sim 96\%$), which is similar to or slightly higher than the 94% of the cloud-free TAI and much higher than the MODIS products in all-sky conditions (50%–64%). In addition, the snow accuracy at the station-based snow depth of ≥ 4 cm shows great improvement for the MODIS products (Table III).

Snow accuracies of the MODIS products and TAI in clear-sky and all-sky conditions associated with different snow depth measurements are evaluated (Fig. 3). In clear-sky conditions, snow accuracy clearly increases for the various snow products when snow depth is greater than 4 cm [Fig. 3(a)]. The daily blended MODIS Terra–Aqua performs the best with an increase

in snow depth. The snow accuracies of different snow products present similar patterns as snow depth increases in all-sky conditions. As expected, the TAI shows the highest accuracy when compared with other products [Fig. 3(b)].

It is interesting to note that, when snow depth is thicker than 10 cm, large fluctuations or even lowering of snow-mapping accuracy occurs. Typically on the TP, snow depth is shallow (≤ 5 cm) and accounts for 86% of station measurements in our study. The distribution of possible thick snow can be very localized and might only be observed at a limited number of stations, i.e., the higher the snow depth values, the fewer the stations recording such high measurements [Fig. 3(c)]. These few valid station measurements of high snow depth would be responsible for the fluctuation of snow accuracy assessments for higher snow depths.

Fig. 4 compares the average snow cover for each year and each basin of the TP using MODIS Terra/Aqua, MODIS Terra–Aqua, IMS, and TAI over 2005–2013. It is clear that the combined MODIS Terra–Aqua underestimates the snow cover because of cloud blockage, while snow cover values between MOD10A2 and IMS ($R^2 = 0.96$), and MOD10A2 and TAI ($R^2 = 0.98$) are highly correlated. This suggests that the new snow product of TAI can retrieve snow cover efficiently. Moreover, the TAI has a higher spatial resolution of 500 m relative to the IMS at 4 km and daily temporal resolution relative to the 8-day MOD10A2.

B. MODIS Terra–Aqua and IMS Combination

Table IV presents the mean annual cloud and snow coverage across the TP from the different snow cover products used in

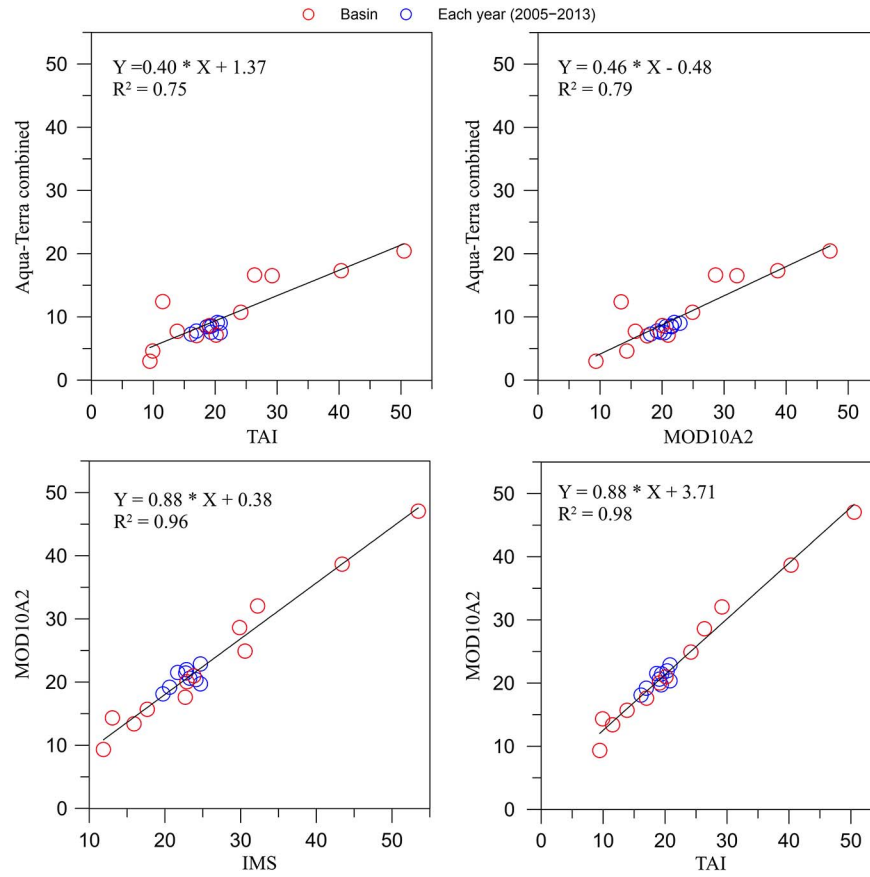


Fig. 4. Comparison of mean snow cover (%) for each year and basin using the daily combined MODIS Aqua–Terra, 8-day MODIS data (MOD10A2), IMS, and daily TAI between 2005 and 2013. The number and name of the 12 basins are shown in Fig. 1.

this study during the period 2001–2013. The mean annual cloud and snow cover values between 2001 and 2013 derived from MOD10A1 are 46.6% (44.1%–49.7%) and 6.2% (5.4%–7.1%), respectively. MYD10A1 exhibits a slightly higher mean annual cloud coverage of 55.1% (50.6%–58.3%) and a slightly lower snow coverage of 4.7% (4.1%–5.3%) relative to MOD10A1. The daily merged MODIS Terra–Aqua provides a product with 37.3% less cloud cover and 8.1% greater snow cover compared with the original MOD10A1 or MYD10A1 alone. However, cloud obscuration in MODIS Terra–Aqua is still a challenge. MOD10A2 yields a mean low cloud residual value of 4.7% (3.9%–6.1%) and high snow cover of 20.6% (18.1%–22.9%), whereas it covers the maximal snow cover extent over an 8-day interval. The cloud-free IMS has an overall higher annual snow cover of 22.5% (19.7%–24.7%). The TAI image has a mean annual snow cover of 19.1% (16.1%–20.8%), which is significantly higher with respect to the daily standard MODIS Terra/Aqua and similar to the 8-day MOD10A2; however, it preserves the high daily temporal resolution and 500-m spatial resolution.

Fig. 5 plots the intra-annual characteristics of clouds and snow cover. Cloud coverage from Terra, Aqua, or Terra–Aqua in January to August is large (> 40%), with the highest coverage in July; clouds decrease in September to the lowest values in October to December. Snow cover in all-sky conditions is less than or near 10% in January to May, lowest in June to September, and slightly higher in October to December. The

snow cover exhibits a reverse pattern when compared with cloud cover in the various months. The cloud transparency of TAI retrieves an obviously high snow cover in October to April. Therefore, the TAI can efficiently suppress cloud cover effects on the MODIS snow cover products.

We also demonstrate snow and cloud cover changes according to the combined product in the Nam Co (lake) Basin of the TP (Fig. 6). Nam Co is the highest altitude large lake in the world, with an altitude of 4725 m and an area of $\sim 2000 \text{ km}^2$ [52], [53]. Many studies use the lake to estimate the water balance of variable snow cover changes in this basin [54], [55]. Daily cloud (snow) coverage values from MODIS Terra and Aqua on March 29, 2008, in the Nam Co Basin are 80.4% (7%) and 65.2% (10%), respectively. The combination of MODIS Terra (morning) and Aqua (afternoon) on this day reveals a lower cloud cover of 58.2% and a greater snow area of 13.1%. After combining MODIS Terra–Aqua and IMS, cloud cover is completely removed, and snow cover (27.5%) increases when compared with 13.1% for the blended MODIS Terra–Aqua product and 26.2% for the IMS. The high spatial resolution of TAI provides clearer results compared with the IMS alone.

In addition, we compare the time series of snow cover changes across the TP using MOD10A2, IMS, and TAI between 2001 and 2013 (Fig. 7). A few MOD10A2 snow cover values are greater than 40%. However, the daily TAI exhibits more fine-grained snow cover fluctuations, particularly high peaks

TABLE IV
MEAN CLOUD AND SNOW COVERAGE (IN PERCENT) ON THE TP FROM THE DAILY MOD10A1, MYD10A1,
DAILY MERGED TERRA–AQUA, 8-DAY MOD10A2, AND DAILY TAI BETWEEN 2001 AND 2013

Year	MOD10A1		MYD10A1		Terra-Aqua		MOD10A2		IMS	TAI
	Cloud	Snow	Cloud	Snow	Cloud	Snow	Cloud	Snow	Snow	Snow
2001	44.9	5.7	-	-	-	-	3.9	19.2	-	-
2002	46.3	6.9	50.6	4.5	33.6	7.6	3.9	22.5	-	-
2003	48.4	5.5	55.8	4.4	39.1	7.3	5.6	18.8	-	-
2004	46.6	6.4	55.3	4.9	37.5	8.3	4.8	20.8	20.9	-
2005	48.9	7.0	57.3	4.9	39.8	9.0	5.5	22.9	24.7	20.8
2006	46.3	6.5	55.8	4.9	36.9	8.5	3.9	21.5	21.7	18.7
2007	44.3	6.0	52.7	4.6	35.4	7.8	4.1	19.2	20.6	17.0
2008	48.5	7.1	57.3	5.3	39.4	9.1	5.7	22.0	22.8	20.3
2009	46.0	6.7	55.5	5.0	36.9	8.6	4.2	21.5	22.8	19.4
2010	45.3	5.4	54.3	4.3	36.3	7.3	4.7	18.1	19.7	16.1
2011	46.2	5.8	55.3	4.4	37.3	7.6	4.3	19.7	24.7	19.4
2012	49.7	5.7	58.3	4.1	40.4	7.5	6.1	20.4	24.1	20.8
2013	44.1	6.5	52.8	5.0	35.4	8.5	4.4	20.6	23.3	19.1
All	46.6	6.2	55.1	4.7	37.3	8.1	4.7	20.6	22.5	19.1

MYD10A1 available from Jul 4, 2002

IMS available from Feb 23, 2004

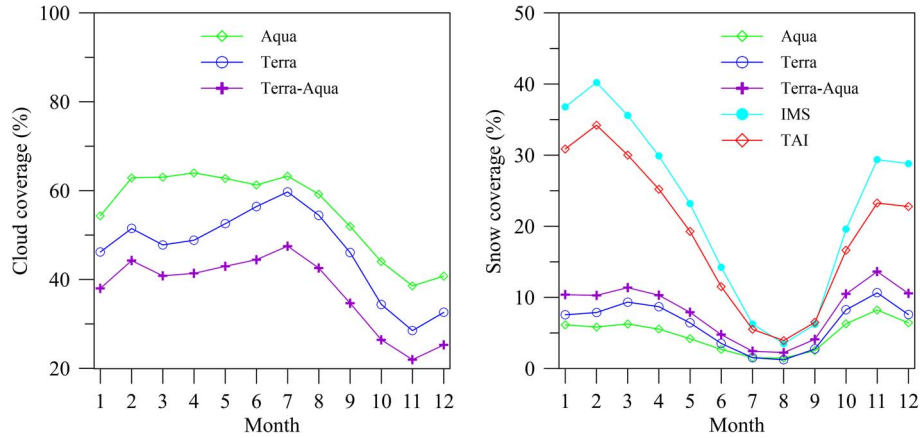


Fig. 5. Mean monthly cloud and snow coverage on the TP from MODIS Terra/Aqua, combined MODIS Terra–Aqua, IMS, and TAI in 2005–2013.

with snow cover $> 50\%$. For example, the highest peak of $> 60\%$ in 2008 is captured by TAI but missed by MOD10A2.

In general, daily cloud coverage across the TP is greater than $\sim 45\%$ according to the daily MODIS Terra/Aqua snow products. Cloud and snow cover can vary greatly by year and region on the TP. The daily combination of MODIS Terra and Aqua with a temporal difference of 3 h can reduce the limited cloud coverage. The snow accuracies of MODIS products in clear-sky and all-sky conditions can improve greatly at the snow depth of ≥ 4 cm relative to ≥ 1 cm. Additionally, the daily composite products could produce data gaps and errors due to the different viewing geometries of MODIS Terra/Aqua [38]. The IMS could overestimate SCA due to poor identification of fractal snow cover (Figs. 4–6). The TAI snow product produced from our algorithm can remove all cloud pixels and recover snow cover pixels in the high mountainous TP. In this algorithm, we only replace the cloud pixels (including no data) in MODIS Terra–Aqua with the IMS and retain other pixels as MODIS values. This could impact the spatial resolution of

the composite product to a significant extent, particularly for massive and consistent cloud cover cases.

V. CONCLUSION

Snow cover images from MODIS sensors are shown to be useful for research involving snow cover. However, obscuring clouds constrain their utility, particularly in high mountainous terrain where cloud obscuration is frequent. In this paper, we have presented a method to remove cloud contamination and retrieve more snow cover pixels by merging daily MODIS 500-m products and the 4-km IMS product to provide a daily 500-m TAI product.

The results from this study show that mean daily cloud obscuration values of 46.6% and 55.1% in MODIS Terra and Aqua, respectively, on the TP between 2001 and 2013 are reduced to 37.3% in the combined Terra–Aqua product. A further combination of the MODIS Terra–Aqua product with IMS yields TAI maps of snow cover at 19.1%. This value is

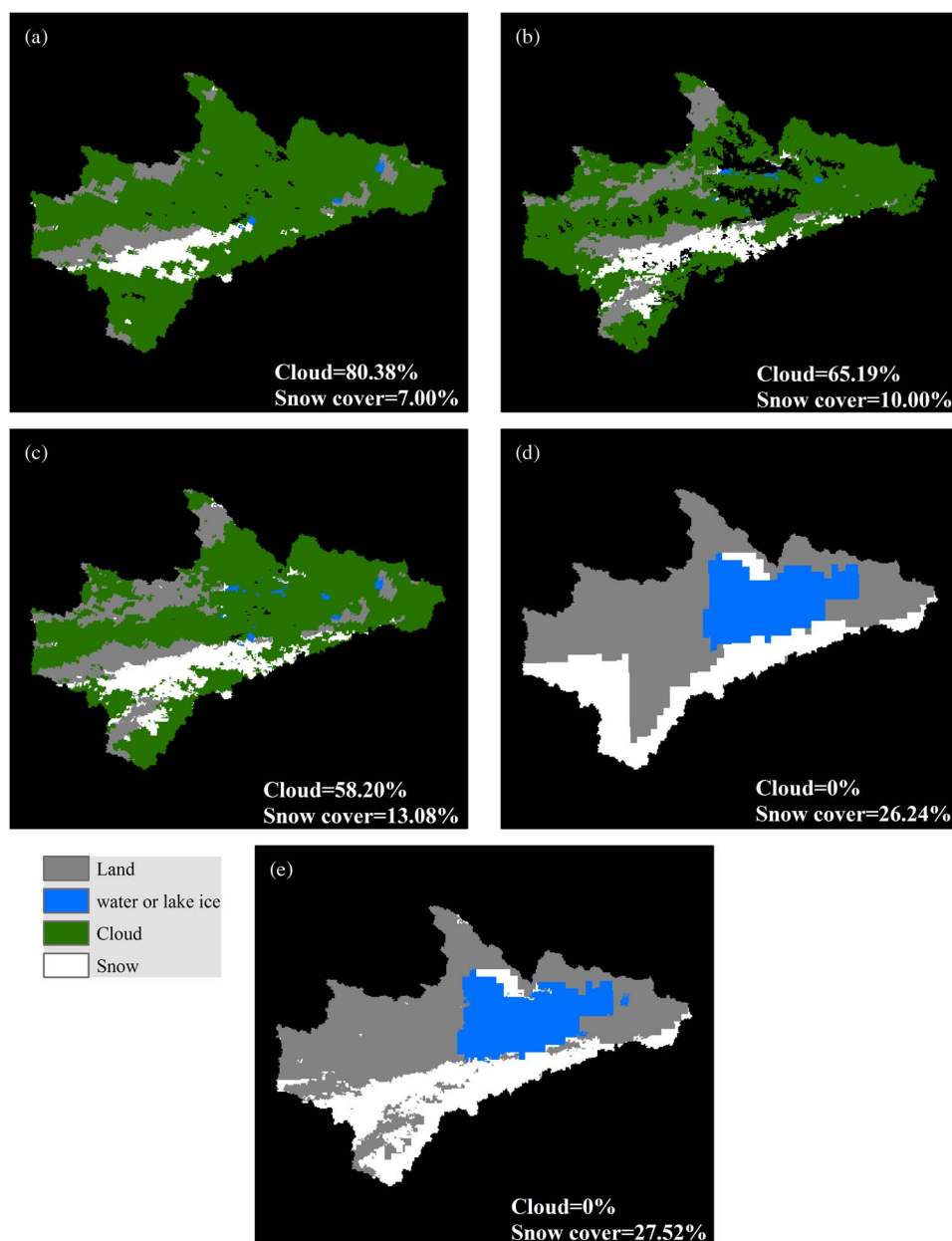


Fig. 6. Example showing cloud and snow cover changes from different snow cover data in the Nam Co Basin. (a) MODIS Terra, (b) MODIS Aqua, (c) daily merged Terra-Aqua, (d) daily IMS, and (e) daily TAI on March 29, 2008.

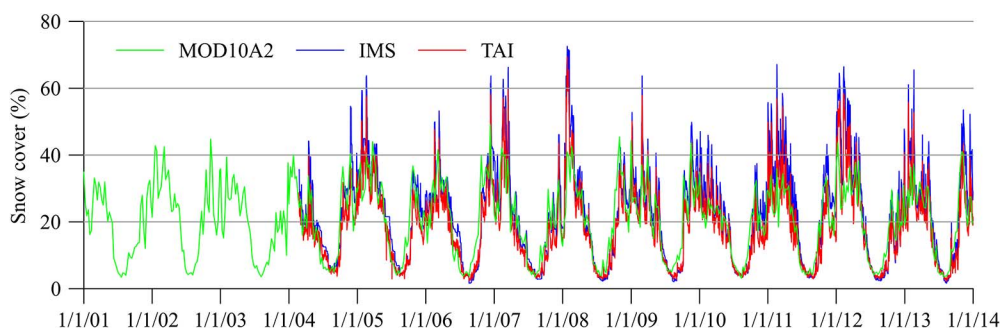


Fig. 7. Time series snow cover variations on the entire TP as observed from MOD10A2, IMS, and TAI between 2001 and 2013.

close to the value derived from the Terra 8-day MOD10A2 product result of 20.6% while in the same time preserving daily observations from the TAI.

ACKNOWLEDGMENT

The authors would like to thank the four anonymous reviewers for their constructional comments that improve this paper.

REFERENCES

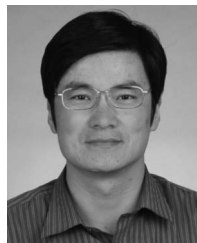
- [1] T. Yao *et al.*, "Different glacier status with atmospheric circulations in Tibetan Plateau and surroundings," *Nat. Clim. Change*, vol. 2, no. 9, pp. 663–667, 2012.
- [2] T. P. Barnett, J. C. Adam, and D. P. Lettenmaier, "Potential impacts of a warming climate on water availability in snow-dominated regions," *Nature*, vol. 438, no. 7066, pp. 303–309, Nov. 2005.
- [3] G. Zhang *et al.*, "Estimating surface temperature changes of lakes in the Tibetan Plateau using MODIS LST data," *J. Geophys. Res., Atmos.*, vol. 119, no. 14, pp. 8552–8567, Jul. 2014.
- [4] C. B. Field, V. R. Barros, D. J. Dokken, K. J. Mach, M. D. Mastrandrea, T. E. Bilir, M. Chatterjee, K. L. Ebi, Y. O. Estrada, R. C. Genova, B. Girma, E. S. Kissel, A. N. Levy, S. MacCracken, P. R. Mastrandrea, and L. L. White, Eds., *Climate Change 2014: Impacts, Adaptation, and Vulnerability. Part A: Global and Sectoral Aspects. Contribution of Working Group I to the Fifth Assessment Report of the Intergovernmental Panel on Climate Change*. Cambridge, U.K.: Cambridge Univ. Press, 2014, IPCC, Stanford, CA, USA.
- [5] Committee on Himalayan Glaciers Hydrology, and Implications for Water Security; Board on Atmospheric Sciences and Climate; Division on Earth and Life Studies; National Research Council, Himalayan Glaciers: Climate Change, Water Resources, and Water Security. Washington, DC, USA: The National Academies Press, 2012, pp. 1–156.
- [6] L. Zhang, F. Su, D. Yang, Z. Hao, and K. Tong, "Discharge regime and simulation for the upstream of major rivers over Tibetan Plateau," *J. Geophys. Res., Atmos.*, vol. 118, no. 15, pp. 8500–8518, Aug. 2013.
- [7] T. Liang *et al.*, "An application of MODIS data to snow cover monitoring in a pastoral area: A case study in Northern Xinjiang, China," *Remote Sens. Environ.*, vol. 112, no. 4, pp. 1514–1526, Apr. 2008.
- [8] C. J. Crawford, S. M. Manson, M. E. Bauer, and D. K. Hall, "Multi-temporal snow cover mapping in mountainous terrain for Landsat climate data record development," *Remote Sens. Environ.*, vol. 135, pp. 224–233, Aug. 2013.
- [9] D. K. Hall, G. A. Riggs, V. V. Salomonson, N. E. DiGirolamo, and K. J. Bayr, "MODIS snow-cover products," *Remote Sens. Environ.*, vol. 83, no. 1/2, pp. 181–194, Nov. 2002.
- [10] A. Frei *et al.*, "A review of global satellite-derived snow products," *Adv. Space Res.*, vol. 50, no. 8, pp. 1007–1029, Oct. 2012.
- [11] R. Barry and T. Y. Gan, *The Global Cryosphere: Past, Present and Future*. Cambridge, U.K.: Cambridge Univ. Press, 2011.
- [12] M. Brodzik and R. Armstrong, *Northern Hemisphere EASE-Grid 2.0 Weekly Snow Cover and Sea Ice Extent, Version 4, [Indicate Subset Used]*. Boulder, CO, USA: NASA DAAC at the National Snow and Ice Data Center, 2013.
- [13] D. A. Robinson, D. K. Hall, and T. L. Mote, *MEaSURES Northern Hemisphere Terrestrial Snow Cover Extent Daily 25 km EASE-Grid 2.0, [Indicate Subset Used]*. Boulder, CO, USA: NASA DAAC at the National Snow and Ice Data Center, 2014.
- [14] W. J. D. van Leeuwen, B. J. Orr, S. E. Marsh, and S. M. Herrmann, "Multi-sensor NDVI data continuity: Uncertainties and implications for vegetation monitoring applications," *Remote Sens. Environ.*, vol. 100, no. 1, pp. 67–81, Jan. 2006.
- [15] A. Huete, K. Didan, W. van Leeuwen, T. Miura, and E. Glenn, "MODIS vegetation indices," *Land Remote Sensing and Global Environmental Change, Remote Sensing and Digital Image Processing*, B. Ramachandran, C. O. Justice, and M. J. Abrams, Eds. New York, NY, USA: Springer-Verlag, 2011, pp. 579–602.
- [16] J. Pulliainen, "Mapping of snow water equivalent and snow depth in boreal and sub-arctic zones by assimilating space-borne microwave radiometer data and ground-based observations," *Remote Sens. Environ.*, vol. 101, no. 2, pp. 257–269, Mar. 2006.
- [17] M. A. Wulder, T. A. Nelson, C. Derksen, and D. Seemann, "Snow cover variability across central Canada (1978–2002) derived from satellite passive microwave data," *Clim. Change*, vol. 82, no. 1/2, pp. 113–130, May 2007.
- [18] Y. Kim, J. S. Kimball, K. Zhang, and K. C. McDonald, "Satellite detection of increasing Northern Hemisphere non-frozen seasons from 1979 to 2008: Implications for regional vegetation growth," *Remote Sens. Environ.*, vol. 121, pp. 472–487, Jun. 2012.
- [19] N. Mazari, A. E. Tekeli, H. Xie, H. O. Sharif, and A. A. El Hassan, "Assessment of ice mapping system and Moderate Resolution Imaging Spectroradiometer snow cover maps over Colorado Plateau," *J. Appl. Remote Sens.*, vol. 7, no. 1, Jul. 2013, Art. ID 073540.
- [20] L. C. Brown, S. E. L. Howell, J. Mortin, and C. Derksen, "Evaluation of the Interactive Multisensor Snow and Ice Mapping System (IMS) for monitoring sea ice phenology," *Remote Sens. Environ.*, vol. 147, pp. 65–78, May 2014.
- [21] X. Liu, X. Jin, and C. Ke, "Accuracy evaluation of the IMS snow and ice products in stable snow covers regions in China," *J. Glaciol. Geocryol.*, vol. 36, no. 3, pp. 500–507, Jun. 2014.
- [22] H. Xie, X. Wang, and T. Liang, "Development and assessment of combined Terra and Aqua snow cover products in Colorado Plateau, USA and Northern Xinjiang, China," *J. Appl. Remote Sens.*, vol. 3, no. 1, Oct. 2009, Art. ID 033559.
- [23] Y. Gao, H. Xie, T. Yao, and C. Xue, "Integrated assessment on multi-temporal and multi-sensor combinations for reducing cloud obscuration of MODIS snow cover products of the Pacific Northwest USA," *Remote Sens. Environ.*, vol. 114, no. 8, pp. 1662–1675, Aug. 2010.
- [24] X. Wang and H. Xie, "New methods for studying the spatiotemporal variation of snow cover based on combination products of MODIS Terra and Aqua," *J. Hydrol.*, vol. 371, no. 1–4, pp. 192–200, Jun. 2009.
- [25] T. Liang *et al.*, "Toward improved daily snow cover mapping with advanced combination of MODIS and AMSR-E measurements," *Remote Sens. Environ.*, vol. 112, no. 10, pp. 3750–3761, Oct. 2008.
- [26] Y. Gao, H. Xie, N. Lu, T. Yao, and T. Liang, "Toward advanced daily cloud-free snow cover and snow water equivalent products from Terra-Aqua MODIS and Aqua AMSR-E measurements," *J. Hydrol.*, vol. 385, no. 1–4, pp. 23–35, May 2010.
- [27] K. P. Paudel and P. Andersen, "Monitoring snow cover variability in an agropastoral area in the Trans Himalayan region of Nepal using MODIS data with improved cloud removal methodology," *Remote Sens. Environ.*, vol. 115, no. 5, pp. 1234–1246, May 2011.
- [28] Z. Tang, J. Wang, H. Li, and L. Yan, "Spatiotemporal changes of snow cover over the Tibetan Plateau based on cloud-removed Moderate Resolution Imaging Spectroradiometer fractional snow cover product from 2001 to 2011," *J. Appl. Remote Sens.*, vol. 7, no. 1, Mar. 2013, Art. ID 073582.
- [29] D. K. Hall, G. A. Riggs, J. L. Foster, and S. V. Kumar, "Development and evaluation of a cloud-gap-filled MODIS daily snow-cover product," *Remote Sens. Environ.*, vol. 114, no. 3, pp. 496–503, Mar. 2010.
- [30] J. Parajka and G. Blöschl, "Spatio-temporal combination of MODIS images—Potential for snow cover mapping," *Water Resour. Res.*, vol. 44, no. 3, Mar. 2008, Art. ID W03406.
- [31] J. Parajka, M. Pepe, A. Rampini, S. Rossi, and G. Blöschl, "A regional snow-line method for estimating snow cover from MODIS during cloud cover," *J. Hydrol.*, vol. 381, no. 3/4, pp. 203–212, Feb. 2010.
- [32] H. Y. Li *et al.*, "Synthesis method for simulating snow distribution utilizing remotely sensed data for the Tibetan Plateau," *J. Appl. Remote Sens.*, vol. 8, no. 9, Jan. 2014, Art. ID 084696.
- [33] J. Tong, S. J. Déry, and P. L. Jackson, "Topographic control of snow distribution in an alpine watershed of western Canada inferred from spatially-filtered MODIS snow products," *Hydrol. Earth Syst. Sci.*, vol. 13, no. 3, pp. 319–326, Mar. 2009.
- [34] H. Zhao and R. Fernandes, "Daily snow cover estimation from Advanced Very High Resolution Radiometer polar pathfinder data over Northern Hemisphere land surfaces during 1982–2004," *J. Geophys. Res., Atmos.*, vol. 114, no. D5, Mar. 2009, Art. ID D05113.
- [35] J. Deng, X. Huang, Q. Feng, X. Ma, and T. Liang, "Toward improved daily cloud-free fractional snow cover mapping with multi-source remote sensing data in China," *Remote Sens.*, vol. 7, no. 6, pp. 6986–7006, May 2015.
- [36] T. H. Painter *et al.*, "Retrieval of subpixel snow covered area, grain size, and albedo from MODIS," *Remote Sens. Environ.*, vol. 113, no. 4, pp. 868–879, Apr. 2009.
- [37] J. Dozier and T. H. Painter, "Multispectral and hyperspectral remote sensing of alpine snow properties," *Annu. Rev. Earth Planet. Sci.*, vol. 32, pp. 465–494, May 2004.
- [38] J. Dozier, T. H. Painter, K. Rittger, and J. E. Frew, "Time-space continuity of daily maps of fractional snow cover and albedo from MODIS," *Adv. Water Resour.*, vol. 31, no. 11, pp. 1515–1526, Nov. 2008.
- [39] K. Rittger, T. H. Painter, and J. Dozier, "Assessment of methods for mapping snow cover from MODIS," *Adv. Water Resour.*, vol. 51, pp. 367–380, Jan. 2013.
- [40] D. K. Hall, G. A. Riggs, and V. V. Salomonson, "Development of methods for mapping global snow cover using Moderate Resolution Imaging Spectroradiometer data," *Remote Sens. Environ.*, vol. 54, no. 2, pp. 127–140, Nov. 1995.
- [41] D. K. Hall and G. A. Riggs, "Accuracy assessment of the MODIS snow products," *Hydrol. Process.*, vol. 21, no. 12, pp. 1534–1547, Jun. 2007.
- [42] Z. Pu, L. Xu, and V. V. Salomonson, "MODIS/Terra observed seasonal variations of snow cover over the Tibetan Plateau," *Geophys. Res. Lett.*, vol. 34, no. 6, Mar. 2007, Art. ID L06706.
- [43] A. G. Klein and A. C. Barnett, "Validation of daily MODIS snow cover maps of the Upper Rio Grande River Basin for the 2000–2001 snow year," *Remote Sens. Environ.*, vol. 86, no. 2, pp. 162–176, Jul. 2003.

- [44] J. Dong and C. Peters-Lidard, "On the relationship between temperature and MODIS snow cover retrieval errors in the Western US," *IEEE J. Sel. Topics Appl. Earth Observ. Remote Sens.*, vol. 3, no. 1, pp. 132–140, Mar. 2010.
- [45] X. Wang, H. Xie, T. Liang, and X. Huang, "Comparison and validation of MODIS standard and new combination of Terra and Aqua snow cover products in northern Xinjiang, China," *Hydrol. Process.*, vol. 23, no. 3, pp. 419–429, Jan. 2009.
- [46] D. K. Hall, V. Salomonson, and G. Riggs, *MODIS/Terra Snow Cover Daily L3 Global 500 m Grid, Version 5*. Boulder, CO, USA: NASA National Snow and Ice Data Center Distributed Active Archive Center, 2006.
- [47] G. Zhang, H. Xie, T. Yao, T. Liang, and S. Kang, "Snow cover dynamics of four lake basins over Tibetan Plateau using time series MODIS data (2001–2010)," *Water Resour. Res.*, vol. 48, no. 10, Oct. 2012, Art. ID W10529.
- [48] K. L. Brubaker, R. T. Pinker, and E. Deviatova, "Evaluation and comparison of MODIS and IMS snow-cover estimates for the continental United States using station data," *J. Hydrometeorol.*, vol. 6, no. 6, pp. 1002–1017, Dec. 2005.
- [49] B. H. Ramsay, "The Interactive Multisensor Snow and Ice Mapping System," *Hydrol. Process.*, vol. 12, no. 10/11, pp. 1537–1546, Aug./Sep. 1998.
- [50] S. S. P. Shen *et al.*, "Characteristics of the Tibetan Plateau snow cover variations based on daily data during 1997–2011," *Theor. Appl. Climatol.*, vol. 120, no. 3/4, pp. 445–453, May 2015.
- [51] National-Ice-Center, *IMS Daily Northern Hemisphere Snow and Ice Analysis at 4 km and 24 km Resolution*. Boulder, CO, USA: National Snow and Ice Data Center, Digital Media, 2008.
- [52] G. Zhang, H. Xie, S. Kang, D. Yi, and S. F. Ackley, "Monitoring lake level changes on the Tibetan Plateau using ICESat altimetry data (2003–2009)," *Remote Sens. Environ.*, vol. 115, no. 7, pp. 1733–1742, Jul. 2011.
- [53] G. Zhang, T. Yao, H. Xie, K. Zhang, and F. Zhu, "Lakes' state and abundance across the Tibetan Plateau," *Chin. Sci. Bull.*, vol. 59, no. 24, pp. 3010–3021, Aug. 2014.
- [54] Y. Wu, H. Zheng, B. Zhang, and L. Lei, "Long-term changes of lake level and water budget in the Nam Co Lake Basin, Central Tibetan Plateau," *J. Hydrometeorol.*, vol. 15, no. 1/2, pp. 1312–1322, Jun. 2014.
- [55] S. Chen *et al.*, "Interrelation among climate factors, snow cover, grassland vegetation, and lake in the Nam Co Basin of the Tibetan Plateau," *J. Appl. Remote Sens.*, vol. 8, no. 1, May 2014, Art. ID 084694.



Jinyuan Yu received the B.S. and M.S. degrees from Southwest University, Chongqing, China, in 2006 and 2009, respectively. She is currently working toward the Ph.D. degree in physical geography in the Institute of Tibetan Plateau Research, Chinese Academy of Sciences, Beijing, China.

She has been a Lecturer with Tibet University, Lhasa, China, since 2009. Her research interest is monitoring environmental changes in the Tibetan Plateau using satellite data.



Guoqing Zhang received the B.S. degree from the East China Institute of Technology, Nanchang, China, in 2002 and the Ph.D. degree in quaternary geology from China University of Geosciences, Beijing, China, in 2011.

He is an Associate Professor with the Institute of Tibetan Plateau Research, Chinese Academy of Sciences, Beijing, and CAS Center for Excellence in Tibetan Plateau Earth Sciences, Beijing. His research interests are lake, snow cover, and glacier changes and their response to climate change in the Tibetan

Plateau using remote sensing data.



Tandong Yao received the B.S. and M.S. degrees in physical geography from Lanzhou University, Lanzhou, China, in 1978 and 1982, respectively, and the Ph.D. degree in physical geography from the University of Chinese Academy of Sciences, Beijing, China, in 1986.

He is a Professor with the Institute of Tibetan Plateau Research, Chinese Academy of Sciences, Beijing, and CAS Center for Excellence in Tibetan Plateau Earth Sciences, Beijing. He has focused on the study of glacier and environment since the 1980s.

He is currently acknowledged internationally as one of the most accomplished scientists in the field of ice core study and glacial fluctuation interpretation.



Hongjie Xie received the B.S. degree from the East China Institute of Technology, Nanchang, China, in 1990, the M.S. degree from the Beijing Research Institute of Uranium Geology, Beijing, China, in 1993, and the Ph.D. degree in geological sciences from the University of Texas at El Paso, El Paso, TX, USA, in 2002.

He is a Professor with the University of Texas at San Antonio (UTSA), San Antonio, TX, and the Founding Director of the Laboratory for Remote Sensing and Geoinformatics, UTSA. His research

interests are in remote sensing and GIS technologies, theories, and applications on surface hydrology and cryosphere.



Hongbo Zhang received the B.S. degree from Shandong Normal University, Jinan, China, in 2010. He is currently working toward the Ph.D. degree in physical geography in the Institute of Tibetan Plateau Research, Chinese Academy of Sciences, Beijing, China.

The topic of his study is hydrological and snow melt modeling in the Tibetan Plateau.



Changqing Ke received the B.S. degree in geography from Shaanxi Normal University, Xi'an, China, in 1993, the M.S. degree in remote sensing and geo-information system from the Cold and Arid Regions Environmental and Engineering Research Institute, Chinese Academy of Sciences (CAS), Lanzhou, China, in 1996, and the Ph.D. degree in remote sensing and geo-information system from Nanjing Institute of Geography and Limnology, Chinese Academy of Sciences (CAS), Nanjing, China, in 1999. He finished his postdoctoral program

at Giessen University, Giessen, Germany, in 2003.

He became a Full Professor with Nanjing University, Nanjing, in 2007. His research interests are remote sensing of cryosphere and climate change.



Ruzhen Yao received the B.S. degree from Lanzhou University, Lanzhou, China, in 2007 and the M.S. degree from the University of Maryland, Baltimore County, Baltimore, MD, USA, in 2011. She is currently working toward the Ph.D. degree in remote sensing in the Institute of Remote Sensing and Digital Earth, Chinese Academy of Sciences, Beijing, China.

The current topic of her study is researching over snow cover and glacier changes mostly on the Tibetan Plateau.